

# Fatigue crack growth prediction of welded joints in low-cycle fatigue region

Takeshi Hanji<sup>1</sup> · Kazuo Tateishi<sup>1</sup> · Nao Terao<sup>1</sup> · Masaru Shimizu<sup>1</sup>

Received: 4 August 2016 / Accepted: 10 July 2017 / Published online: 8 August 2017  
© International Institute of Welding 2017

**Abstract** Low-cycle fatigue is one of the failure modes in steel structures during earthquakes. With a focus on crack growth in the low-cycle fatigue region, this study developed a fatigue crack growth curve and verified its applicability to crack growth prediction in welded joints. Fatigue crack growth tests under highly plastic conditions were performed using compact tension specimens with side grooves. The results indicate that the crack growth rate in the low-cycle fatigue region correlates with the cyclic J-integral range, which can be calculated using finite element analysis. Additionally, the results for both plain steel and weld metal were distributed in the same region within a narrow band. Based on the results, a formula for the fatigue crack growth rate under large cyclic strains was proposed. Low-cycle fatigue tests were then performed on welded joints to clarify their crack growth behavior, and the crack growth observed in these tests was compared with the crack growth calculated using the proposed formula. The calculation results were found to be in relatively good agreement with the experimental results, verifying the applicability of the formula.

**Keywords (IIW Thesaurus)** Fatigue crack growth rate · Low-cycle fatigue · Cyclic J-integral range · Welded joints

---

Recommended for publication by Commission XIII - Fatigue of Welded Components and Structures

---

✉ Takeshi Hanji  
hanji@civil.nagoya-u.ac.jp

<sup>1</sup> Nagoya University, Nagoya, Japan

## 1 Introduction

Low-cycle fatigue, which is a type of fatigue damage due to large cyclic strains, is one of the primary failure modes of steel structures during earthquakes. After the Hyogo-ken Nanbu earthquake in 1995, low-cycle fatigue failure was observed in steel bridge piers [1]. Additionally, it has been revealed that low-cycle fatigue cracks occur mostly in welded joints because of the strain concentration around the weld. Therefore, a fatigue life prediction method for welded joints in the low-cycle fatigue region should be established to prevent the collapse of steel structures during earthquakes.

Basically, fatigue life is defined as the sum of the crack initiation and propagation lives. The Coffin–Manson law, which was derived from previous research on the crack initiation life, is a well-known prediction model that represents the crack initiation life as a function of the plastic strain amplitude [2, 3]. Based on the concept of the Coffin–Manson law, the authors have established a prediction model for use in the extremely low-cycle fatigue region. The model is applicable to not only plain steel but also weld metal and the heat-affected zone (HAZ) [4].

Regarding the crack propagation life in the high-cycle fatigue region, previous studies have reported that the crack growth rate varies linearly with the stress intensity factor range on log–log scales; this is widely known as the Paris–Erdogan model [5]. However, this approach cannot be applied to the low-cycle fatigue region, because large-scale plastic deformation occurs around crack tips in this region.

Under high-plasticity conditions, previous studies have indicated that the J-integral calculated from the area under a load–displacement hysteresis loop, called the cyclic J-integral range, correlates with the crack growth rate [6, 7]. Furthermore, researchers have attempted to apply the cyclic J-integral concept to cracks under extremely high-strain

conditions [8]. Here, the method of calculating the cyclic J-integral used in previous studies can be used only for particular types of specimen configurations, making it difficult to apply directly to welded joints.

Several other parameters have been also proposed for use in predicting crack growth in the low-cycle fatigue region. An equation describing the relationship between the cyclic crack tip opening displacement [9] and the crack growth rate has been proposed [10]. Additionally, it has been demonstrated that the crack growth rate is related to the strain intensity factor range proposed based on the stress intensity factor concept [11–13]. However, the applicability of these parameters to cracks in welded joints has not yet been thoroughly investigated.

In this study, with a focus on crack growth in the low-cycle fatigue region, a prediction model for crack growth was developed, and its applicability to a crack in welded joints was verified through fatigue tests.

## 2 Fatigue crack growth tests

### 2.1 Specimen

Fatigue crack growth tests were conducted using compact tension (CT) specimens, as shown in Fig. 1a. The specimen configurations and dimensions were in accordance with ASTM standard E1820-08. An artificial notch was made in the specimen to act as the origin of the crack. As shown in Fig. 1b, side grooves were also cut into both sides of the specimen to ensure a straight crack front in the thickness direction. The crack propagated from the notch along the grooves as a result of cyclic loading.

Three types of specimens were prepared to compare crack growth behavior in plain materials and weld metal. The specimens were cut from the centers of steel plates of JIS-SM490A and JIS-SM400A (structural steels of 490 and 400 N/mm<sup>2</sup> classes) with thicknesses of 18 and 19 mm, respectively, and a butt-welded joint, as shown in Fig. 2.

**Fig. 1** Specimens (unit: mm)

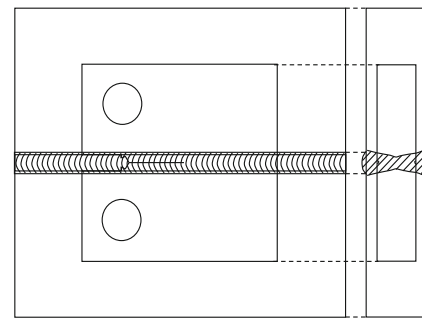
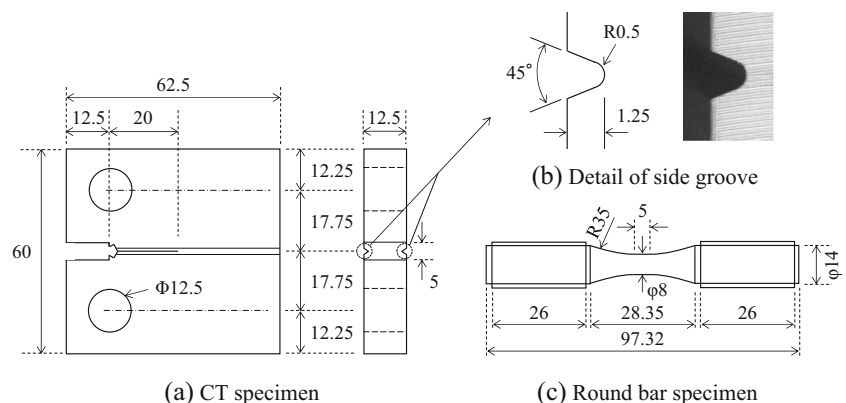


**Fig. 2** Specimen for weld metal

The plate thickness for all specimens was 12.5 mm. The butt-welded joint was made using submerged arc welding with an X-groove (two welding passes at a welding current of 600 A, a welding voltage of 38 V, and a welding speed of 40 cm/min). Welding material was JIS Z 3183 S501-H. In the specimen from the welded joint, the crack propagated through the weld metal.

The results of the tensile test are shown in Fig. 3, and the mechanical properties of the materials used for the specimens are given in Table 1. The tensile tests were conducted using the round-bar specimens shown in Fig. 1c, which were cut from the steel plates and the weld metal in the welded joint. In the test, axial strain was computed from diametral strain measured with a diametral extensometer [14].

### 2.2 Testing methods

Figure 4 shows the test setup. Each specimen was fixed to a testing machine and loaded under displacement control. A clip gauge was attached to the specimen to measure the displacement along the loading axis. The range of fluctuation of the displacement was controlled during the test. The test matrix is given in Table 2. In each test, the minimum displacement was set to be 0 mm except in case 7, in which the displacement range was the same as in case 5 but the minimum value was

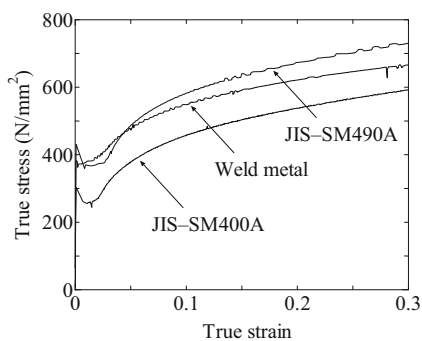


Fig. 3 Tensile test results

Table 1 Mechanical properties of materials

Materials	Yield stress (N/mm <sup>2</sup> )	Tensile strength (N/mm <sup>2</sup> )	Elongation (%)
JIS-SM400A	302	442	42
JIS-SM490A	430	552	43
Weld metal	383	510	45

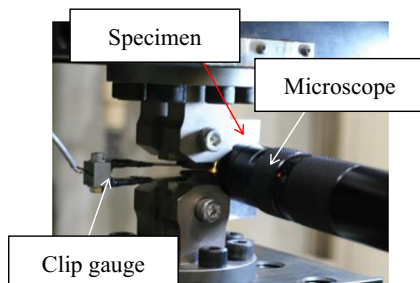


Fig. 4 Test setup

changed to 1.5 mm to investigate the effect of the mean displacement. The loading speed ranged from approximately 0.001 to 0.05 mm/s.

The crack length was measured at regular intervals using a microscope while the maximum displacement was applied to the specimen. The crack measurement was initiated when the crack grew to approximately 1 mm from the notch. The test continued until the crack reached a length of approximately 12–15 mm. Subsequently, the specimen was broken by elastic cyclic deformation.

Table 2 Test matrix

Case	1	2	3	4	5	6	7	8	9	10	11
Material	JIS-SM400A			JIS-SM490A			Weld metal				
Displacement range (mm)	0.8	1.5	3.0	0.8	1.5	3.6	1.5	0.4	0.8	1.5	3.0
Minimum displacement (mm)	0	0	0	0	0	0	1.5	0	0	0	0

### 2.3 Test results

Figure 5 shows examples of load–displacement hysteresis loops for cases 1, 2, and 3. In the graph, the maximum load of each cycle continually decreased because of the crack growth. This tendency became more noticeable as the displacement range increased. In addition, inflection points were observed in the unloading process, implying that the crack surfaces gradually come into contact.

Figure 6 shows an example of a crack tip observed from the side surface of the specimen. This figure reveals that the crack propagated straight along the side groove. The relationships between the crack length and the number of cycles in cases 1, 2, and 3 are shown in Fig. 7. The crack growth rate increased in proportion to the displacement range.

A photograph of one of the fracture surfaces after the test is shown in Fig. 8. In general, the crack front becomes convex because the plane strain condition is dominant around the center of the plate in the thickness direction and the crack grows more rapidly at the center of the plate than at its surface. As shown in Fig. 8, the location of the crack front was almost same throughout the thickness direction because of the side groove. These cracking patterns were observed in all specimens.

## 3 Fatigue crack growth rate formula in low-cycle fatigue region

### 3.1 Calculation of cyclic J-integral range

Finite element analysis was used to calculate the cyclic J-integral range at the cracks in the specimens. In this study, the cyclic J-integral was used to evaluate the crack growth rate in the specimen.

#### 3.1.1 Definition of cyclic J-integral range

The J-integral proposed by Rice [15] is a path-independent integral that represents the strain energy release rate of non-linear elastic materials. In this study, the cyclic J-integral range

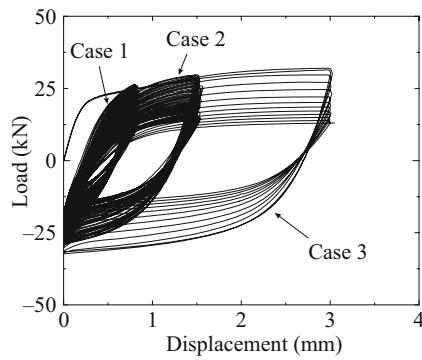


**Fig. 5** Load–displacement hysteresis loop

$\Delta J$  was defined as the range of fluctuation of the J-integral from the minimum to the maximum load points of the loading process, as shown in Fig. 9. The cyclic J-integral range is calculated as:

$$\Delta J = \int_{\Gamma} \left( W' dy - \Delta T \frac{\partial \Delta u}{\partial x} ds \right) \quad (1)$$

$$W' = \int_0^{\Delta \varepsilon_{ij}} \Delta \sigma_{ij} d\Delta \varepsilon_{ij} \quad (2)$$

where  $W'$  is the range of strain energy density,  $\Delta T$  is the range of traction vector,  $\Delta u$ ,  $\Delta \sigma$ , and  $\Delta \varepsilon$  are the ranges of displacement vector, stress, and strain in the loading process, respectively.

### 3.1.2 Analysis methods

Elasto-plastic finite element analysis was conducted using Abaqus 6.13. Figure 10a shows the three-dimensional analysis model and its boundary conditions. Taking advantage of the symmetry of the specimens, a quarter model with eight-node solid elements was used. The minimum element size was approximately 0.5 mm around the crack tip. The side grooves were included in the model. A model without side grooves was also created to investigate their effect. Furthermore, a two-dimensional analysis model under the plane strain assumption was created using four-node elements, as shown in

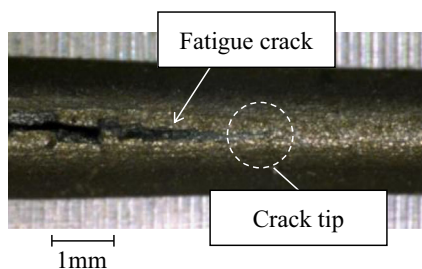


**Fig. 6** Crack tip observed from side surface

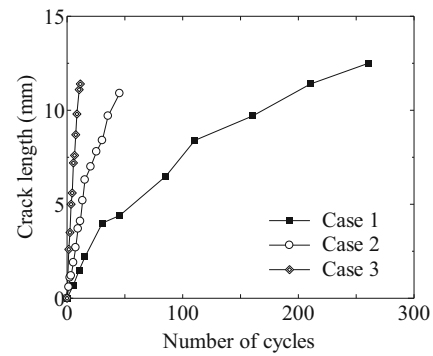


**Fig. 7** Crack length vs number of cycles

Fig. 10b. For the boundary conditions, the displacement in the vertical direction was fixed at the ligament parts. Rigid elements were used to connect the loading point and the specimen. A cyclic displacement was applied to the loading point. To simulate crack closure, rigid contact elements were arranged on the opposite side of the crack surface, which experienced no friction.

In the weld metal specimen, the base and weld metal regions, which were determined based on the etched surface of the specimen, were modeled individually, as shown in Fig. 10a. Different constitutive equations were assigned to each region. A multi-linear constitutive law based on the tensile tests shown in Fig. 3 and the kinematic hardening model was applied. Young’s modulus and Poisson’s ratio were 200 kN/mm<sup>2</sup> and 0.3, respectively.

Because it has been generally assumed that residual stress is released as a result of large plastic deformations, no residual stress was considered in this analysis.

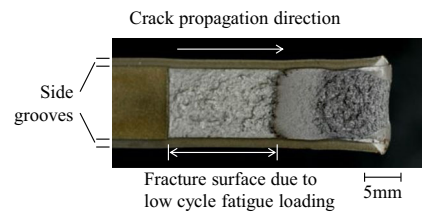


**Fig. 8** Fracture surface

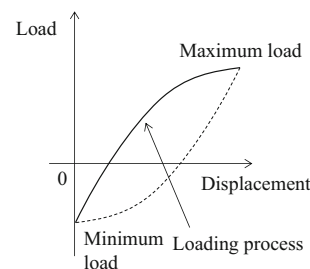
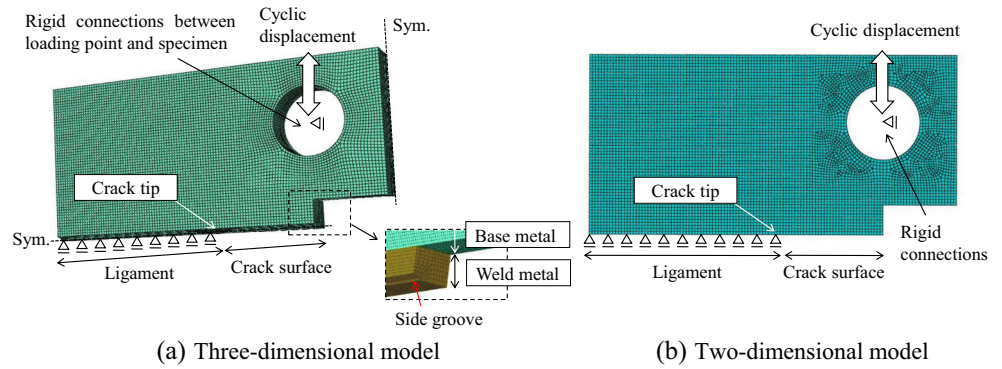


**Fig. 9** Calculation concept of cyclic J-integral range

**Fig. 10** Analysis model and boundary conditions



3.1.3 Analysis results

The analytical load–displacement relationship in the three-dimensional model is shown in Fig. 11 together with the experimental results. The analytical and experimental results were in good agreement with each other. This verifies that the finite element model can accurately represent the actual behavior of the specimen.

Figure 12 shows the J-integral at the side surface and the thickness center of the specimen. The J-integral at the side surface in the three-dimensional model with the side groove was computed at a section of 0.5 mm inside from the bottom of the groove. As shown in Fig. 12a, the side grooves caused a

significant increase in the J-integral at the side surface, meaning that the groove caused the stress–strain conditions at the surface to be similar to the plane strain condition. As shown in Fig. 12a, b, the model with the groove indicates that the J-integrals at the side surface and the thickness center are nearly equal. These tendencies were almost similar regardless of element sizes from 0.1 to 0.5 mm. This result can be supported by the crack growth pattern in the specimen, where the crack front is almost the same throughout the thickness direction.

Figure 12b also includes the results of the two-dimensional model. There is little difference between the J-integrals of the two- and three-dimensional models. Therefore, in this study, the cyclic J-integral calculated using the two-dimensional model was used to evaluate the crack growth rate in the test.

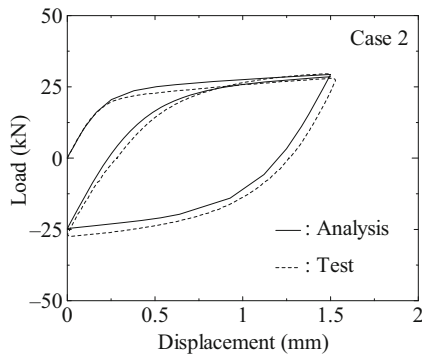
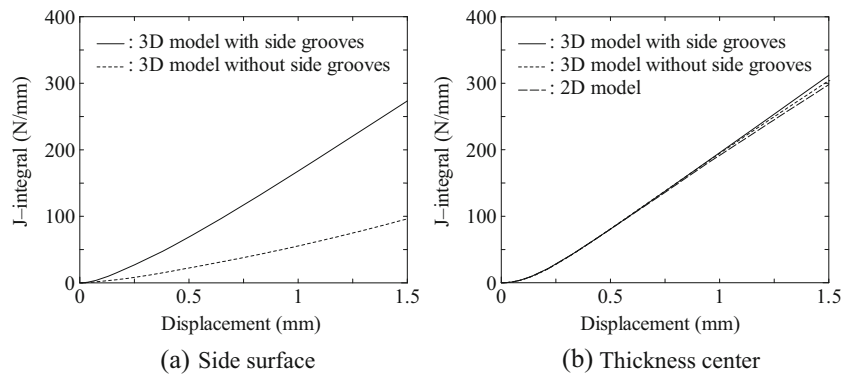


**Fig. 11** Comparison of load–displacement hysteresis loop

3.2 Relationships between crack growth rate and cyclic J-integral range

The cyclic J-integral range was determined for any crack length in the specimen using the following procedure: First, several models with crack lengths ranging from 2 to 16 mm at 2-mm intervals were created. Then, the cyclic J-integral range was calculated for each model during the loading process shown in Fig. 9 while applying the cyclic displacement for 1.5 cycles. Here, the path independence of the cyclic J-integral range was confirmed by assessing several integration paths

**Fig. 12** Comparisons of J-integral at side surface and thickness center



surrounding the crack tip, as shown in Fig. 13, and the average of the resulting values was used in this study. As a result of this analysis, the relationship between the cyclic J-integral range and the crack length was obtained, as shown in Fig. 14. Based on the relationship, the cyclic J-integral range at an arbitrary crack length was calculated.

Figure 15 shows the relationship between the crack growth rate  $da/dN$  measured during the tests and the cyclic J-integral range  $\Delta J$  calculated analytically. Figure 15a–c shows the results for each material, and all of the results are summarized in Fig. 15d. The curves are each located within a relatively narrow area regardless of the applied displacement range and mean displacement. Additionally, all plots were distributed in the same area, as shown in Fig. 15d, meaning that the cyclic J-integral range correlates with the crack growth rate regardless of the material. Based on the results, the following formula can be derived assuming that the relationship yields a straight line on log–log scales:

$$\frac{da}{dN} = 9.6 \times 10^{-6} (\Delta J)^{1.67} \quad (3)$$

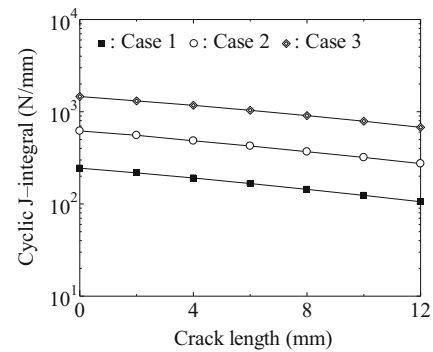
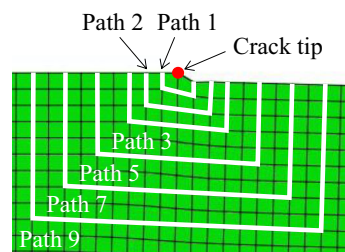
## 4 Fatigue crack growth prediction in welded joints

### 4.1 Low-cycle fatigue tests of welded joints

Low-cycle fatigue tests were conducted using corner welded joints [16]. The crack growth of the corner welded joint was predicted to confirm the applicability of the proposed crack growth curve.

Figure 16 shows the configurations and dimensions of the corner welded joint. In the specimen, two plates were connected with a single-bevel-groove weld to simulate a longitudinal weld between the flange and web plates in a steel bridge pier. The specimen has a weld root with a length of approximately 8 mm.

**Fig. 13** Path independence of cyclic J-integral range



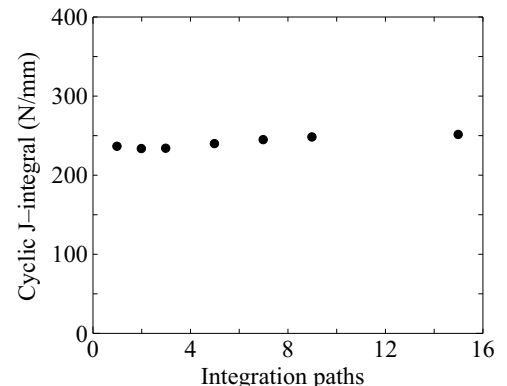
**Fig. 14** Cyclic J-integral range vs crack length

Figure 17 shows the testing method. A crack was initiated from the weld root due to cyclic bending deformation. Photographs of an observed crack are shown in Fig. 18. The photographs were taken at the side surface of the specimen at regular intervals. As shown in the figure, the crack propagated in the thickness direction with changing its direction. The test was continued until the specimen was failed. Further details of this test can be found in reference [16].

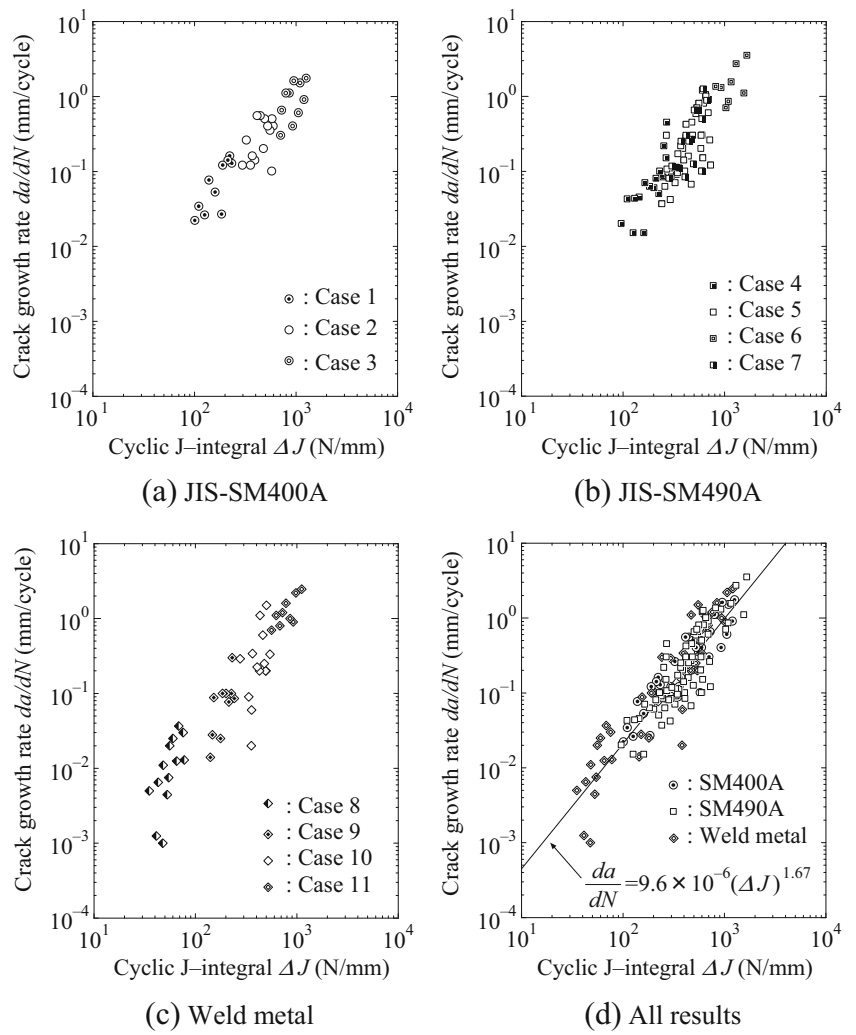
### 4.2 Analysis methods

Figure 19 shows the analysis model and its boundary conditions. A two-dimensional analysis model under the plane strain assumption was created using four-node elements. This model also includes a pair of loading devices. For the boundary conditions, the center of the upper hole, where a pin connection was applied during the test, was fixed, and a cyclic displacement was applied to the bottom hole. Rigid elements were used to connect the loading and fixing points to the specimen.

The mesh around the crack tip is shown in Fig. 19. The crack path was modeled based on the actual crack shape obtained in the experiment. The weld root and crack were simulated with double contact nodes, where the contact



**Fig. 15** Crack growth rate vs cyclic J-integral range



condition with no friction was applied. A square grid mesh with an element size of 0.2 mm was arranged around the crack tip.

Young’s modulus and Poisson’s ratio were 200 kN/mm<sup>2</sup> and 0.3, respectively. As in a previous study [16], the base and weld metal regions were modeled individually, and different constitutive equations were assigned to

each region. The stress–strain relationship was the multi-linear constitutive law, and the kinematic hardening model was used.

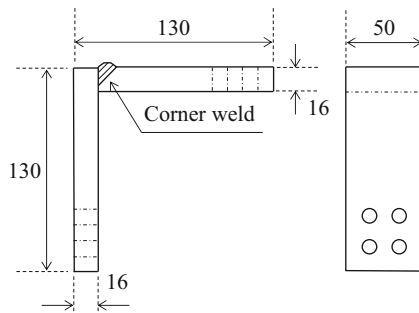


**Fig. 16** Corner welded joint (unit: mm)

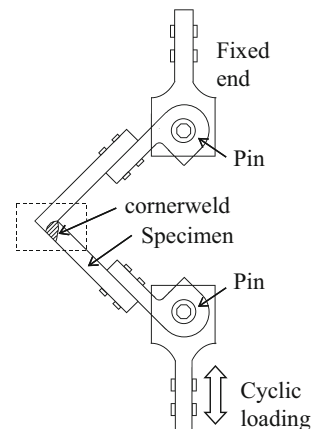


**Fig. 17** Testing method

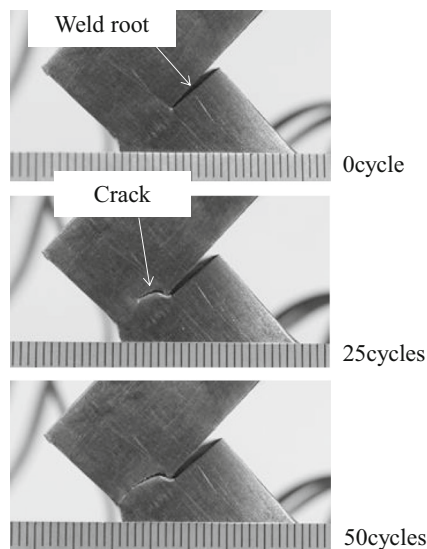


**Fig. 18** Crack observations

To obtain the relationship between the cyclic J-integral range and the crack length, several models with different crack lengths were created. The cyclic J-integral range in each model was calculated using the method described in Chap. 3.

### 4.3 Fatigue crack growth predictions

The crack growth in the test was estimated based on the cyclic J-integral range from the analysis and the proposed formula given in Eq. (3) by the following steps: (a) At first, some models which have different crack lengths were created, and a relationship between the crack length  $a$  and the cyclic J-integral  $\Delta J$  was obtained. (b) Next, the initial crack length was defined and its cyclic J-integral was calculated based on the relationship in step (a). (c)

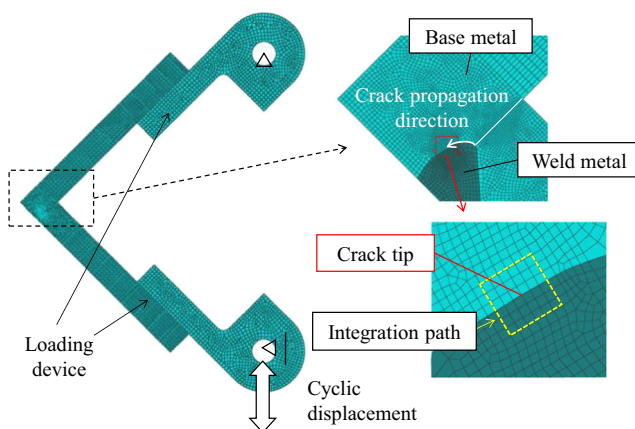


**Fig. 19** Analysis model and boundary conditions

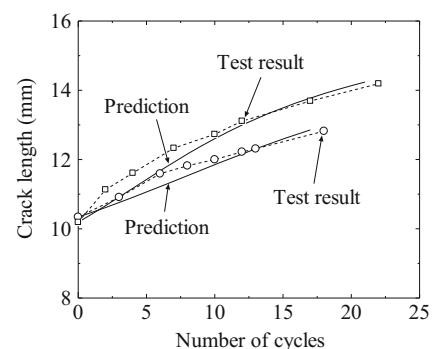
According to Eq. (3), crack growth length  $da$  due to 1 loading cycle ( $dN = 1$ ) was calculated. (d) Then, the crack length  $a$  was updated to  $a + da$ , and again, its cyclic J-integral was calculated based on the relationship in step (a). (e) The crack growth length  $da$  was re-calculated by Eq. (3). The steps from (d) to (e) were repeated to the final crack length.

Figure 20 shows the prediction results. The crack length is defined as the summation of the length of the weld root face and the crack, which were measured along the root and crack. In the prediction, the initial crack length was set to 10 mm, which is the crack length after a growth of 2 mm from the root tip, because it was difficult to properly distinguish the crack from the weld root in the early stages of crack growth. The crack growth observed in the tests is also shown in the graph.

The predicted and observed crack growths were in good agreement, and the difference between them was less than 0.5 mm. This demonstrates that the crack growth of the corner welded joints can be predicted using the cyclic J-integral range and the proposed crack growth formula in the low-cycle fatigue region.

## 5 Conclusions

This study established a crack growth curve in the low-cycle fatigue region for plain steel and weld metal, which represents the relationship between the crack growth rate and the cyclic J-integral range. In addition, the crack growth in the tested corner welded joints was estimated using the cyclic J-integral range and the proposed curve. The predictions agreed well with the experimental results. Therefore, it was concluded that the crack growth in welded joints in the low-cycle fatigue region can be accurately predicted using the proposed curve with the cyclic J-integral range.



**Fig. 20** Crack growth prediction in welded joints



**Acknowledgements** The authors acknowledge the support of Chubu Electric Power Co., Inc. in Japan and express our sincere gratitude to Dr. Matsumura at The Takigami Steel Construction Co., Ltd. in Japan for specimen fabrications.

## References

- Okashita K, Ohminami R, Michiba K, Yamamoto A, Tomimatsu M, Tanji Y, Miki C (1997) Investigation of the brittle fracture at the corner of P75 rigid-frame pier in Kobe Harbor Highway during the Hyogoken-nanbu Earthquake. *J JSCE* 591/I-43:243–261 (in Japanese)
- Manson SS (1953) Behavior of materials under conditions of thermal stress, NACA technical note, 2933
- Coffin LF Jr (1954) A study of the effects of cyclic thermal stresses on a ductile metal. *Trans ASME* 76:931–950
- Tateishi K, Hanji T, Minami K (2006) A prediction model for extremely low cycle fatigue strength of structural steel. *Int J Fatigue* 29(5):887–896
- Paris P, Erdogan F (1963) A critical analysis of crack propagation laws. *Trans ASME J Basic Eng* 85(4):528–533
- Dowling NE, Begley JA (1976) Fatigue crack growth during gross plasticity and the J-integral. *ASTM STP* 590:82–103
- Dowling NE (1976) Geometry effects and the J-integral approach to elastic-plastic fatigue crack growth. *ASTM STP* 601:19–32
- Tanuma Y, Kobayashi H (2002) Study on ultra-low-cycle-fatigue crack growth characteristics of high strength steel. *J Struct Constr Eng* 553:105–112 (in Japanese)
- Shih CF (1981) Relationships between the J-integral and the crack opening displacement for stationary and extending cracks. *J Mech Phys Solids* 29(4):305–326
- Schweizer C, Seifert T, Nieweg B, Hartrott P, Riedel H (2011) Mechanisms and modelling of fatigue crack growth under combined low and high cycle fatigue loading. *Int J Fatigue* 33(2): 194–202
- Haigh JR, Skelton RP (1978) A strain intensity approach to high temperature fatigue crack growth and failure. *Mater Sci Eng* 36(1): 133–137
- Kamaya M, Kawakubo M (2012) Strain-based modeling of fatigue crack growth—an experimental approach for stainless steel. *Int J Fatigue* 44:131–140
- Kamaya M (2015) Low-cycle fatigue crack growth prediction by strain intensity factor. *Int J Fatigue* 72:80–89
- Bui-Quoc T, Biron A (1978) Comparison of low-cycle fatigue results with axial and diametral extensometers. *Exp Mech*:127–133
- Rice JR (1968) A path independent integral and the approximate analysis of strain concentration by notches and cracks. *J Appl Mech* 35:379–386
- Hanji T, Park JE, Tateishi K (2014) Low cycle fatigue assessments of corner welded joints based on local strain approach. *Int J Steel Struct* 14(3):579–587